Title

The end of ice I

Journal

Proceedings of the National Academy of Sciences of the United States of America, 116(49)

ISSN

0027-8424

Authors

Moberg, Daniel R
Becker, Daniel
Dierking, Christoph W
et al.

Publication Date

2019-12-03

DOI

10.1073/pnas.1914254116

Peer reviewed

The end of ice I

Daniel R. Moberg[a], Daniel Becker[b,1], Christoph W. Dierking[b,1], Florian Zurheide[b,1], Bernhard Bandow[c,2], Udo Buck[d], Arpa Hudait[e], Valeria Molinero[e,3], Francesco Paesani[a,3], and Thomas Zeuch[b,3]

[a]Department of Chemistry and Biochemistry, University of California San Diego, La Jolla, CA 92093; [b]Institut für Physikalische Chemie, Universität Göttingen, D-37077 Göttingen, Germany; [c]Computer Center, Max-Planck-Institut für Sonnensystemforschung, D-37077 Göttingen, Germany; [d]Max-Planck-Institut für Dynamik und Selbstorganisation, D-37077 Göttingen, Germany; and [e]Department of Chemistry, The University of Utah, Salt Lake City, UT 84112-0850

Edited by Pablo G. Debenedetti, Princeton University, Princeton, NJ, and approved October 3, 2019 (received for review August 16, 2019)

The appearance of ice I in the smallest possible clusters and the nature of its phase coexistence with liquid water could not thus far be unraveled. The experimental and theoretical infrared spectroscopic and free-energy results of this work show the emergence of the characteristic hydrogen-bonding pattern of ice I in clusters containing only around 90 water molecules. The onset of crystallization is accompanied by an increase of surface oscillator intensity with decreasing surface-to-volume ratio, a spectral indicator of nanoscale crystallinity of water. In the size range from 90 to 150 water molecules, we observe mixtures of largely crystalline and purely amorphous clusters. Our analysis suggests that the liquid–ice I transition in clusters loses its sharp 1st-order character at the end of the crystalline-size regime and occurs over a range of temperatures through heterophasic oscillations in time, a process without analog in bulk water.

nanoscopic water | phase transitions | IR spectroscopy | molecular simulations

The emergence of macroscopic water properties and anomalies can be studied in a systematic manner in clusters. The characteristic hydrogen-bond network of ice I was first observed in the 1980s in the supersonic expansion of water vapor, and the critical onset size for ice I in clusters was estimated to be between 200 and 1,000 water molecules (1). Only in the present decade have infrared (IR) spectroscopic techniques advanced to the point where the appearance of characteristic ice I signatures can be observed with precise size resolution, first in neutral clusters with about $n = 275$ molecules (2) and later in La^{3+} doped cationic clusters at about $n = 375$ (3). These sizes represent upper limits for the onset size and, so far, could not help in distinguishing predictions of the smallest cluster that forms ice I in molecular simulations, which range from above $n = 123$ and below $n = 293$ (4), above $n = 90$ (5), and between $n \approx 100$ and $n = 137$ (6). Therefore, the smallest size of water clusters that crystallize into ice I on cooling has not yet been established in experiments. This situation is in contrast to the progress made since the 1990s in unraveling the structures of smaller $(H_2O)_n$ clusters through size-selective experiments assisted by ab initio calculations (7–11). The transition from 2-dimensional to 3-dimensional structures in $(H_2O)_6$ and dynamical aspects of melting-like transitions in $(H_2O)_8$ and $(H_2O)_9$ are now quite well understood (12–16). In some special cases, larger individual isomers (17) or cluster sizes with exceptionally stable configurations were determined (18–21). However, all these ordered isomers are specific to an individual size or a narrow size range. They are not representative of macroscopic water or ice properties. The large remaining uncertainty with regard to the onset of crystallization in neutral water clusters is not only due to technical limitations, like the selection of size in experiments and the accuracy of modeling predictions of cluster energies. With increasing cluster size arises a critical influence parameter in both experiment and simulation, whose importance was not sufficiently recognized in the past: the rate at which the initially supercooled liquid clusters are cooled when they begin crystallizing (6). Cooling too rapidly, or insufficient residence times, can result in vitrified amorphous clusters (6, 22), which explains the dependence of the observed onset size on experimental conditions like stagnation pressure in supersonic expansions (13, 23). A related issue is present in search algorithms for global minima structures, where strategies are developed to circumvent barriers blocking isomerization coordinates to local and global minima (13). In turn, the quality of predicted energies and spectroscopic signatures of identified minima highly depends on the applied level of theory (13). We can therefore state 3 challenges that must be considered when aiming to determine the smallest cluster size that stabilizes ice I. First, selectivity toward size and structure in the experiment; 2nd, control of cluster dynamics and relaxation to the energetically most stable structures in experiment and molecular simulations; and 3rd, the development of efficient water models that reliably predict both the energetics and spectroscopic features of crystalline and noncrystalline water clusters. Significant progress has been made in all 3 fields in recent years. In the present study, we combine these advances in experiment and modeling for a comprehensive characterization of the IR spectroscopic signatures and the thermodynamic and kinetic constraints of the emergence of ice I and the nature of its phase coexistence with liquid water in the smallest possible clusters.

In the experiment, a molecular beam of clusters was generated in a supersonic expansion of a water–argon mixture

Significance

How small can a water cluster be and still stabilize ice I, the macroscopic crystal polymorph? What is the nature of coexistence between ice and liquid in small clusters? In this work, we show that the smallest water clusters that can sustain ice contain only around 90 water molecules. Our experimental and theoretical analysis suggests that the melting transition in these small droplets is very different from macroscopic water and our everyday experience. When cooled slightly below their freezing temperature, water clusters with less than ∼150 molecules can oscillate in time between the liquid and crystalline state. These results can be significant to understand the state of water confined in proteins and other materials.

Author contributions: U.B., V.M., F.P., and T.Z. designed research; D.R.M., D.B., C.W.D., F.Z., B.B., and A.H. performed research; B.B. and U.B. analyzed data; and D.R.M., V.M., F.P., and T.Z. wrote the paper.

The authors declare no competing interest.

This article is a PNAS Direct Submission.

See Commentary on page 24383.

[1]D.B., C.W.D., and F.Z. contributed equally to this work.

[2]Present address: High Perfomance Computing, Gesellschaft für wissenschaftliche Datenverarbeitung mbH Göttingen (GWDG), D-37077 Göttingen, Germany.

[3]To whom correspondence may be addressed. Email: tzeuch1@gwdg.de, valeria.molinero@utah.edu, or fpaesani@ucsd.edu.

This article contains supporting information online at https://www.pnas.org/lookup/suppl/doi:10.1073/pnas.1914254116/-/DCSupplemental.

First published November 4, 2019.

through a conical nozzle. Such expansions result in final cluster temperatures from around 150 K down to about 40 K (13). It only recently became possible to simulate in detail the gas and aggregation dynamics in this type of experiment for conditions enabling crystallization in water clusters consisting of around 200 water molecules (23). The results of these numerical simulations and earlier experimental observations (13) suggest the combination of low stagnation pressure and a slow argon-seeded molecular beam for achieving low cooling rates at temperatures below 200 K, where molecular simulations predict that crystallization occurs in clusters with less than a few hundred molecules (4, 6). In this work, we observed the onset of crystallization in a weak expansion of 1 bar stagnation pressure and a reservoir temperature of 343 K that yielded 0.3 mol fraction of water in argon as the carrier gas. Fig. 1 illustrates the 3 characteristic zones for the aggregation and gas dynamics in the conical nozzle, together with estimated temperatures and cooling rates derived from the detailed numerical simulations by Gimelshein et al. (23) for a neon-seeded expansion resulting in a similar size distribution.

The temperature dropped rapidly in the entrance zone, establishing the size distribution. The highest cooling rates in this region approached 1 K/ns, where temperatures reached between 270 and 220 K. The molecular beam was established at around 50 μm from the nozzle entrance, where the temperatures have cooled to around 200 K and the cooling rates have slowed to around 0.5 K/ns. The final cluster temperatures of around 150 K were approached with a further decrease of gas density at around 250 μm, where the cooling rates have dropped below 0.1 K/ns. The validity of the final temperature estimates for this type of expansion has been demonstrated by tracking isomer population changes in the range of 40 to above 150 K (13); see, e.g., the case of the melting-like transition of the water nonamer (15). The water clusters in the molecular beam were then singly tagged with Na atoms when passing through a pickup cell. The sodium atoms enabled their soft, fragmentation-free photoionization near the threshold of 3.2 eV (385 nm) using ultraviolet light from a commercial dye laser. The ionized clusters were size-selectively detected by time-of-flight mass spectrometry. The positive, size-resolved IR action signal resulted from cluster excitation with radiation from a tunable IR laser 80 to 100 ns before photoionization. The action effect exploited the increased abundance of solvated Na atoms with low ionization energy in the heated clusters and the high fraction of undissolved Na atoms with ionization energies above 3.5 eV (24). More details on the method are given in ref. 2 and *Materials and Methods*. We used the characteristic red shift of the absorption maximum of the hydrogen-bonded OH stretch oscillators to detect crystalline clusters in the molecular beam (2, 3). Additionally, we introduce in this work a signature in the free OH stretch band, known for ice surfaces (25), as an independent indicator for emerging crystallinity in clusters.

Recently developed simulation techniques for obtaining IR spectroscopic signals of aqueous systems complement these experimental efforts. Molecular dynamics simulations with many-body potentials (MB-MD) for water have been shown to accurately reproduce structural, thermodynamic, and dynamical properties of aqueous systems across both system size and phases (26). In particular, the fully flexible atomistic many-body potential for water, MB-pol (27–29), predicts vibrational spectra that compare favorably with experimental results for systems ranging from small water clusters to the bulk phase (30, 31). Here, we used MB-MD simulations with the MB-pol potential energy function for water in the canonical (constant number, volume, and temperature [NVT]) ensemble to equilibrate clusters, followed by MB-MD simulations in the microcanonical (constant number, volume, and energy [NVE]) ensemble to calculate IR spectra from time-correlation functions of the system dipole moments. This applies for all predicted cluster energies and IR spectra in this study. The initial structures of clusters with n = 70 to 120 were determined with a parallel evolutionary algorithm (PEA) (5), while those of crystallized clusters with $n > 120$ were obtained by cooling clusters modeled with the many-body monatomic water model mW (32) at the same rate as in our experiment. We classified each water molecule in a cluster as either "liquid-like" or "ice I-like" using the CHILL+ algorithm (33). More details on the molecular simulation methods are given in *Materials and Methods* and *SI Appendix*.

The size-resolved experimental and simulated IR spectra of clusters with about 60 to 200 water molecules are shown in Fig. 2. The experiments at slow cooling conditions revealed the

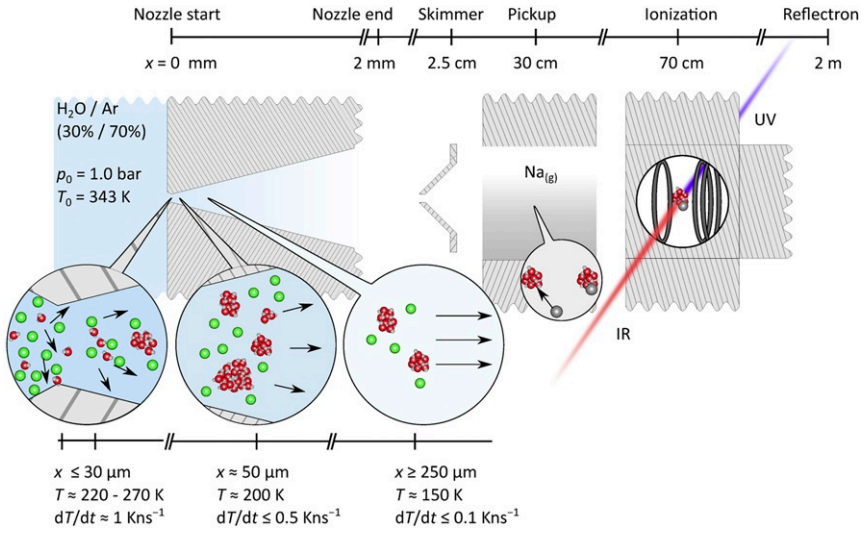

Fig. 1. Scheme of experimental setup with focus on aggregation dynamics in the conical nozzle. For this nozzle, a detailed numerical simulation (23) has predicted the cluster size distribution, the cluster temperatures, and the cluster velocities as a function of distance from the nozzle start. From these quantities, the estimated cooling rates are derived. The validity of the prediction is shown in its ability to capture the final size distribution and its shift by initial temperature variation (23). The estimated final temperature is around 150 K. More details on the simulation and the temperature approximation are given in *Materials and Methods*. UV, ultraviolet.

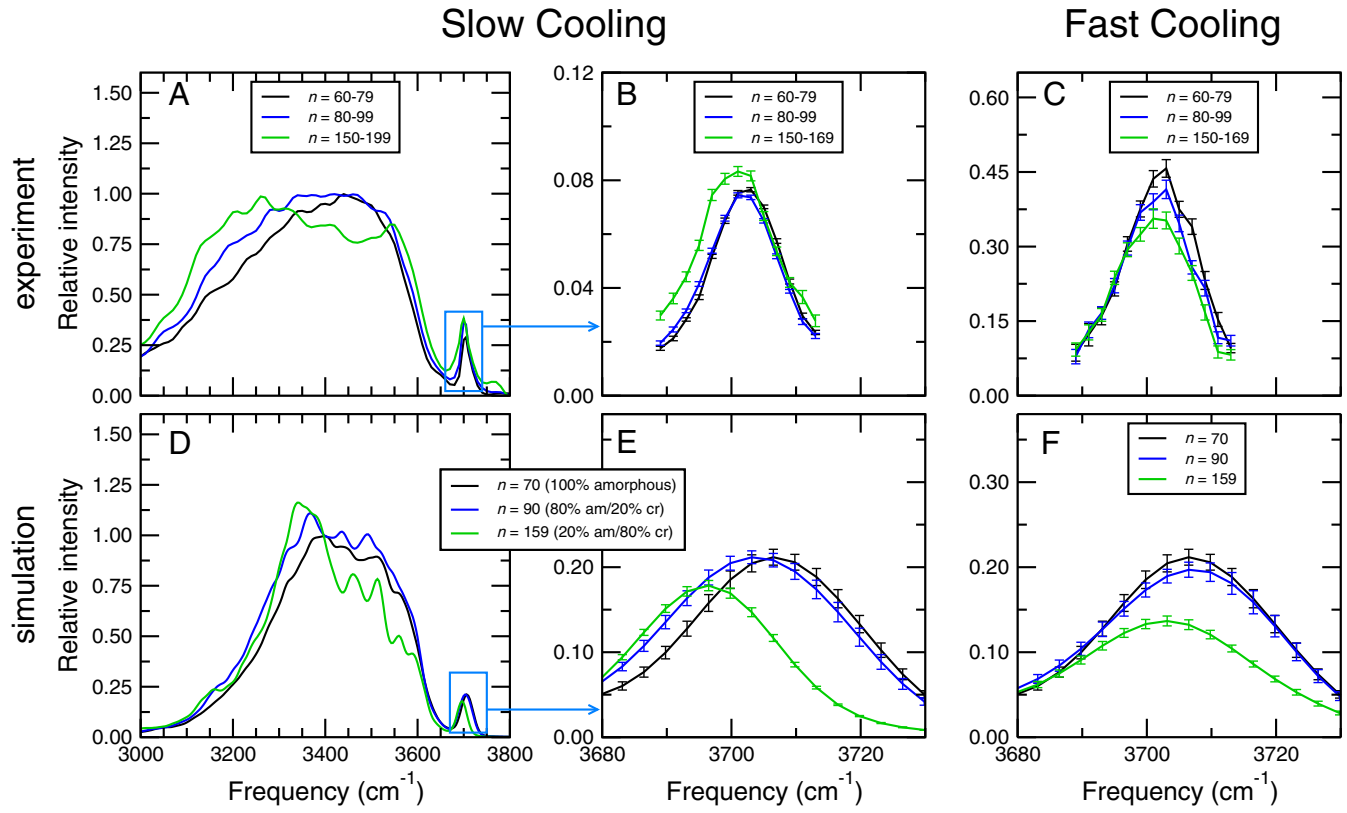

Fig. 2. Experimental (*A*-*C*) and simulated (*D*-*F*) IR spectra of $(H_2O)_n$ clusters produced under slow cooling conditions showing the emerging peak at ∼3,300 cm^{-1}, a signature of crystallinity in the bonded OH stretch band at cluster sizes slightly below n = 100 (*A* and *D*). The ∼3,700 cm^{-1} free OH stretch band also displays signs of crystallinity, namely, the increase in intensity in the experimental spectrum, and the general redshift of the peak (*B* and *E*). Note that all free OH band intensities are normalized against the integrated intensities of the bonded OH stretch band. *C* and *F* show the contrasting size evolution of the free OH stretch band under fast cooling conditions producing solely amorphous clusters. The simulated spectra for n = 90 and n = 159 in *D* and *E* are weighted linear combinations of the IR spectra of amorphous and crystalline clusters (i.e., prepared with rapid cooling and slow cooling conditions, respectively). It is important to note that, particularly at smaller cluster sizes, the crystalline clusters are not purely crystalline, but are composed of a crystalline core with an amorphous surface layer. The error bars represent a 1σ confidence interval.

emergence of a shoulder in the low-frequency region of the bonded (Fig. 2*A*) and free OH (Fig. 2*B*) stretch bands for clusters with 90±10 molecules (see also *SI Appendix*, Figs. S1–S3, where the significance of the red shifts between n = 70 and 90 is readily apparent). The maximum intensity of the bonded OH stretch band for cluster sizes above n = 150 has shifted to values below 3,300 cm^{-1}, indicating the dominance of internal H_2O molecules in an "ice I-like" configuration, as observed in previous studies (2, 3). The shoulder in the free OH stretch band has sharply increased in this size range, and there was a surprising gain in relative intensity normalized to the bonded OH intensity. Typically, a decrease is expected as the surface-to-volume ratio decreases with cluster size, and, therefore, the relative number of free OH oscillators at the surface should decrease accordingly. This was what we observed in a control experiment (Fig. 2*C*) at high stagnation pressure under fast cooling conditions, which produced amorphous water clusters of sizes up to n = 400 (13). In that case, the relative free OH stretch intensity decreased, and there was no intensity gain below 3,700 cm^{-1}. A similar comparison of slow and fast cooling conditions for the bonded OH band also showed the onset of a relative signal gain around 3,200 cm^{-1} to start for clusters containing 80 to 100 water molecules under slow cooling conditions (*SI Appendix*, Fig. S2). We therefore have ample experimental evidence that this size range marks the lower limit for the existence of ice I in clusters. We note that the intensity gain of surface oscillators with decreasing surface-to-volume ratio at the onset of crystallization represents an indicator of nanoscale water crystallinity, here observed for n = 90 to 150. That may also occur for larger cluster sizes (3) noting that the free OH band was not systematically analyzed in this respect in that study.

The early onset of crystallization in the present experiments at 90±10 water molecules clearly supports Bandow and Hartke's (5) prediction that water clusters with a crystalline ice I core become energetically competitive at around n = 90. Consequently, we used the structures from their work as initial structures for simulating with MB-pol the IR spectra in the bonded and free OH stretch regions for n = 120 and below. We modeled the experimental IR spectra as arising from mixtures of crystalline and amorphous clusters to capture the onset size of emerging crystalline signatures, which are centered around 3,200 cm^{-1} (Fig. 2 and *SI Appendix*, Fig. S1), the intensity maximum of larger purely crystalline clusters (4). The simulated IR spectra of neutral clusters qualitatively captured the transition from amorphous to crystalline water clusters and the resulting red shift in the bonded IR spectrum (Fig. 2*D*). Only amorphous clusters were used to generate the spectrum in Fig. 2*D* at n = 70, while ratios of amorphous to crystalline clusters of 4:1 and 1:4 were used for n = 90 and n = 159, respectively. This assumed shift in ratio is consistent with the trend of the simulated free energies in this size range, which are discussed below. The missing intensity below 3,300 cm^{-1} (belonging to fully coordinated and single-donor double-acceptor [DAA] molecules) in the simulated spectra is attributed to a Fermi resonance between the OH-stretching and HOH-bending modes not properly captured in the simulation (32). The underpredicted bond strength of DAA oscillators may cause the missing intensity at low

frequencies and may also cause the broader simulated band of the corresponding free OH oscillator molecules (Fig. 2 *E* and *F*). The simulations correctly predicted the gain in intensity below 3,700 cm^{-1} for the free OH band for slow cooling conditions (Fig. 2*E*) that lead to crystallization and the loss of intensity above 3,700 cm^{-1} for fast cooling conditions producing solely amorphous clusters (Fig. 2*F*). Additionally, the simulations predicted the experimentally observed gain in relative free OH stretch intensity when crystalline clusters were admixed with amorphous clusters. Compared to the experiment, the effect was a bit more pronounced at n = 90 and less pronounced at n = 159. However, quantitative agreement cannot be expected, as intensities are difficult to predict, and the experimental spectra are a result of not-necessarily linear action spectroscopy. A very important point here is that the increase of the relative free OH band intensity is a strong and unambiguous effect in this size range. It is related to the presence of a crystalline core, which increases the number of surface oscillators by about 50% for n = 90 compared to amorphous clusters, as derived from the results of Bandow and Hartke (5). Since the intensity evolution of the free OH band clearly deviated between slow and fast cooling conditions (Fig. 2 *B* and *C*) in the analyzed size range, we can rule out that the simultaneous red shift in the bonded OH band, the established indicator of crystallinity in water clusters (2, 3, 22), is related to a different structural effect.

To rationalize the IR spectroscopic results, we analyzed the relative stability of crystalline and amorphous water cluster structures, spanning from slightly below the early onset size for crystallization observed in this work (n = 90) to the delayed onset sizes (up to n = 293) in earlier studies (2, 3, 13), noting that indications for emerging crystallinity around n = 100 were reported for protonated water clusters (34). We calculated the free energies with MB-pol using the quasiharmonic approximation (35, 36) on energies and vibrational normal modes obtained from cluster structures identified by Bandow and Hartke (5) as starting points for n = 70, 90, and 120 and by simulations with mW for all larger sizes (6).

Fig. 3 shows the difference in free energy $F_{\mathrm{crystalline}}$-$F_{\mathrm{amorphous}}$ of optimized amorphous and crystalline clusters from n = 70 to 293 computed at 100 and 150 K. Although there was, as expected, a temperature dependence for the amorphous to crystalline transition, we found that already for n = 90, the crystallized and purely amorphous clusters were equally stable within the error bars at T = 100 and 150 K. We note that the discrimination between amorphous and ice-like clusters was challenging for n = 70 due to the small crystalline core of "ice I-like" cluster isomers and distributed molecules in "ice I-like" geometry in amorphous clusters (snapshots in Fig. 3 and *SI Appendix*, Fig. S4). At larger cluster sizes, crystalline structures became gradually more stable, and the corresponding "ice I-like" signal was much more pronounced in the IR spectra. Snapshots of the simulated crystalline clusters in Fig. 3 also illustrate the growing ice-like core in the analyzed size region. These free-energy calculations are in good agreement with the Gibbs–Thomson analysis of the size-dependent equilibrium melting temperature of water clusters, which predicts T_{m} = 140 ± 8 K for $n = 90$ and T_{m} = 128 ± 9 K for $n = 70$ (6). We assigned the experimental IR spectra above $n = 90$ to mixtures of amorphous, liquid-like, and crystalline clusters based on the indistinguishable free energies of the amorphous and crystallized clusters with $n = 90$ in the simulations, the presence of fully crystalline (intensity increase centered around 3,200 cm^{-1}) and amorphous (high remaining intensity above 3,400 cm^{-1}) features in the experimental spectra and the agreement between the spectra in the experiment and molecular simulations in Fig. 2. The presence of mixtures was consistent with molecular heat capacities from calorimetry experiments in this size and temperature range (38). The free-energy calculations of Fig. 3, together with the Gibbs–Thomson analysis of ref. 6, paint a picture consistent with the experimental and simulated results outlined in Fig. 2: The formation of a crystalline core becomes more and more energetically unfeasible below n = 100, resulting in amorphous clusters. The disconnected nature and negligible fraction of molecules with ice I order in the n = 70 clusters, together with the crossing between the glass-transition

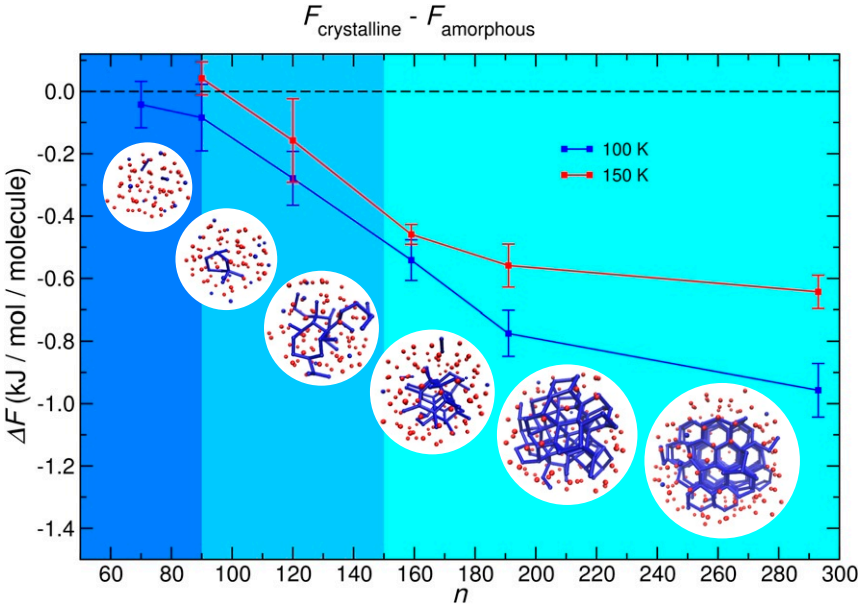

Fig. 3. Simulated difference in molar free energy per molecule of amorphous and crystalline water clusters in the size range from n = 70 to n = 293. For $n \leq 120$, initial structures were taken from Bandow and Hartke (5). For larger clusters, mW was used to nucleate clusters of varying sizes used as initial structures. Evaporation was not observed in the simulations, consistent with our previous simulations (6) and the high free-energy barrier of evaporation reported in ref. 37. Background shading indicates approximately the regions for which ice I is unstable (dark blue); amorphous and ice I clusters coexist through heterophasic oscillations in time (medium blue); and clusters crystallize to ice I through a well-defined 1st-order transition (light blue). Snapshots of each simulated size of crystalline cluster are also included for comparison.

temperature T_g and the T_m of the clusters for that size, is consistent with the experimental analysis, indicating that the end of ice I occurs for clusters with $n = 90 \pm 10$ water molecules.

The growing stability of crystalline structures at $T = 100$ and 150 K above the region near $n = 140$ explains previous experimental assignments of onset sizes above $n = 200$ (2, 3, 13). This, and the coexistence of crystallized and amorphous clusters above the onset size, point to delicate thermodynamic and kinetic constraints for ice nucleation in the size range from $n = 60$ to $n = 300$ studied here. The interdependence of crystallization barriers and critical cooling rates was studied in simulations with the mW water model by Johnston and Molinero (6). They found that clusters with n around 400 could be crystallized at a cooling rate of 0.1 K/ns, but those with $n = 159$ molecules required cooling rates slower than 0.05 K/ns to nucleate ice at 150 K (6). More intriguingly, the simulations revealed that at $n = 137$, the free-energy barrier for the transition between all liquid and crystallized clusters at 150 K was comparable to the thermal energy, and the clusters oscillated in time between the amorphous and crystallized states with a small ice I core surrounded by disordered water (6). Ice–liquid phase coexistence through oscillations has also been recently reported for water in nanoscale confinement (39). Multiple heterophasic oscillations of the $n = 137$ cluster occurred along hundreds of nanoseconds (6), and the transitions become even faster for smaller clusters (39). The assignment of the IR spectra of clusters with 90 to 150 water molecules in Fig. 2 and *SI Appendix*, Fig. S1 to mixtures strongly supports that oscillations between crystallized and amorphous configurations were also present in the experiment. The presence of mixtures, together with the obvious presence of the forward reaction (liquid to crystal), supports the presence of the backward reaction under quasithermal equilibrium conditions around 150 K in the beam (Fig. 1). Note that molecular heat capacities in line with the presence of mixtures of solid and liquid clusters, although interpreted as a glassy state, were measured under equilibrium conditions in a similar size and temperature range for anionic water clusters (38). These previous experiments and the observation of liquid-like and crystalline mixtures in the present study clearly support the existence of ice–liquid oscillations in water, a phenomenon that signals the coda of the 1st-order liquid–ice I transition for small-sized systems and that was first predicted 3 decades ago by Berry and coworkers for Lennard–Jones clusters (40).

The experiments and simulations of this study give unambiguous evidence that the end of ice I occurs for clusters with $n = 90 \pm 10$ through the validation and use of the free OH band as an independent surface indicator for nanoscale crystallinity. Most significantly, the comprehensive analysis of this work interlinks in a consistent manner experimental and theoretical concepts for studying microscopic water properties of the past 30 years, which now can be seen in a common perspective. Just a few of the many examples are the links of the free OH band to the interior structure for clusters (this work and ref. 5) and for bulk water (25); the influence of cooling rates on onset sizes for crystallization (6, 13, 23) and, closely related, the onset of crystallization in neutral (1, 2, 13) and ionic clusters (3, 34); and the complementary character of calorimetry experiments with anionic clusters (38) and the neutral cluster results of this work. Bolstered by this high degree of consistency, the present study identifies the size range of $n = 90 \pm 10$ water molecules as a boundary that demarcates the behavior of water clusters as "macromolecules" with multiple size-dependent isomers and the birth of the ice I-phase characteristic of bulk water. Our analysis indicates further that in clusters with less than 150 water molecules, the nature of the liquid–ice I transition loses its sharp 1st-order character and occurs over a range of temperatures through heterophasic oscillations in time. The oscillations between liquid and ice states result from the small number of molecules in the clusters and have no analog in bulk water. However, this state may exist in materials or substances like proteins that contain nanoconfined water (39). Heterophasic oscillations are a yet-hypothesized concept for nanoscale phase-change dynamics that may find future applications. In general, the results of this work lend increased predictive power to state-of-the-art molecular simulation techniques, which are indispensable tools for studying the role of structures and phase-transition dynamics of nanoscale water in, e.g., biological, atmospherical, geophysical, and astrophysical environments.

Materials and Methods

Below, we provide methodological information on the experiments and the molecular simulations performed in this work. Further details and additional figures are provided in *SI Appendix*.

Experimental Setup and IR Spectra Generation. We have described the molecular-beam generation and the subsequent experimental steps in the main text. Here, we provide details on the laser systems and the generation of the IR action spectra shown in Fig. 2 and *SI Appendix*, Figs. S1–S3. For the IR excitation of the clusters, we used a tunable IR optical parametric oscillator/optical parametric amplifier system (LaserVision) pumped by a solid-state laser (Continuum Powerlite 8000). Subsequent photoionization was carried out with 80- to 100-ns delay at 385 nm with a solid-state laser (Continuum Powerlite 9010) and a pumped dye laser (Sirah Cobra Stretch). More details are found in ref. 24. Both lasers were operated at 10 Hz, but the Q switch of the IR laser was only at 5 Hz. Thus, per second, 5 mass scans with IR laser on and 5 scans with IR laser off were alternately recorded. The signal was the IR-induced relative ion signal gain. The complete IR spectra in Fig. 2 and *SI Appendix*, Fig. S1 were taken with 10-cm^{-1} step width for the bonded and 5 cm^{-1} around the free OH stretch bands. The free OH stretch spectra were taken with 2-cm^{-1} step width (Fig. 2 *B* and *C* and *SI Appendix*, Fig. S3). The bandwidth of the IR laser was 3.7 cm^{-1}. The spectra in Fig. 2*A* and *SI Appendix*, Fig. S1 were averaged over 3 scans and smoothed by averaging 3 neighboring points (25%, 50%, and 25%) 3 times. The trends in the averaged spectra were seen in each individual scan, and the onset became significant for the size range 80 to 99 (*SI Appendix*, Fig. S1). To more precisely pinpoint the onset size, we recorded the signal intensity with high averaging in the region of maximum intensity gain of crystalline clusters (3,180 cm^{-1}) and near the absorption maximum of amorphous clusters (3,420 cm^{-1}) for slow and fast cooling conditions. The results are shown and discussed in *SI Appendix*, Fig. S2. Also, the IR spectra for the narrow free OH stretch band under slow cooling conditions were recorded with much higher averaging, resulting in the small error margins shown in *SI Appendix*, Fig. S3. We note that the Na influence on the IR spectra was negligible for the here-analyzed size range and already limited for clusters containing only 20 water molecules (17).

Simulation of Aggregation and Gas Dynamics. The general estimation of the final cluster temperature is based on the energy balance model of Buck and colleagues (15). Measuring the average cluster size and the kinetic energy after the expansion provides key information for obtaining the cluster temperature. The detailed formulae are given in ref. 15. The results of this method were recently confirmed for the cluster production of a neon–water mixture in a comprehensive simulation by a hybrid Lagrange–Eulerian approach which contains all necessary processes, including the coalescence of clusters and evaporation of monomers (23). The mass difference of a factor of 2 between neon in the simulation and argon in the present experiment leads to a slower beam, slightly reducing the cooling rates compared to the simulation. The simulations show that the nozzle geometry determines the shape of the cluster temperature profiles (and thus the cooling rates as a function of the distance from the nozzle entrance), while gas composition and stagnation pressure determine the final temperature. Variation of the latter shifts the temperature profiles parallel to the position axis (23). The temperature gradients and cooling rates (derived from the simulated temperature gradients and cluster velocities) are highest near the nozzle entrance; they drop with the decreasing gas density and become very low (<0.1 K/ns) when the clusters slowly approach their final temperatures. Therefore, very low cooling rates are achieved below 200 K for final temperatures of around 150 K, according to the estimate of Buck's energy balance model. We note that final temperatures predicted by this model for different expansions are in very good agreement with the measured and simulated shifts in the relative populations of the cage and book isomer of $(H_2O)_6$ (13). For the present argon experiment, the

estimated final temperature was around 150 K, which is consistent with the trends from detailed simulations for neon-seeded expansions at higher stagnation pressure. For the helium-seeded expansion, the estimated final temperatures were around 50 K, drastically increasing the cooling rates above 150 K.

Preparation of Initial Clusters with mW. Liquid water droplets of size n = 159, 191, and 293 water molecules were prepared and equilibrated for 1 ns at 298 K. Before performing the cooling simulations of these water droplets, we estimated the freezing temperature of maximum crystallization rate for a droplet of radius r, $T_f^{max}(r) = T_f^{bulk,\ max} - K_f(r - d)$, where $T_f^{bulk,\ max}$ is the freezing temperature of bulk mW water, the constant K_f = 20 K· nm, and $d = 0.6$ nm is a correction to the radius of the particle (6). Based on the estimated freezing temperature, 3 independent cooling simulations for each droplet size were performed in the temperature range from $T_f^{max}(r)$ + 20 and $T_f^{max}(r) - 20$, with a cooling rate of q_{max} listed in *SI Appendix*, Table S1. Each of these crystallized configurations was analyzed using CHILL+ (33), and the configuration with the highest fraction of ice I (hexagonal and cubic ice) was chosen to build the initial system for simulations with the MB-pol model. The selected cooling rates ensure that the clusters are always in thermal equilibrium (6). All simulations of water nanodroplet crystallization using mW water were performed with LAMMPS (41). The constant cooling simulations were performed in the NVT ensemble. The temperature was controlled with a Nosé–Hoover thermostat with relaxation time of 1 ps (42–44). The equations of motion were integrated by using the velocity Verlet algorithm and a 10-fs timestep.

Simulations with the Atomistic Polarizable MB-pol Water Molecule. MB-MD simulations using the MB-pol potential energy function for water were performed to compute the IR spectra of the ice clusters. These clusters were obtained either through mW simulations or PEA. To acquire more starting cluster configurations, as discussed in the main text, crystalline clusters were extracted from equilibrated ice I bulk systems to create clusters of the desired size ±5 water molecules. Amorphous clusters were obtained by first melting existing crystalline clusters at 300 K in the NVT ensemble for 100 ps before extremely rapidly freezing to the desired temperature. Whether using experimental or mW-derived initial configurations, the amorphous and crystalline clusters were equilibrated in the NVT ensemble for 1,000 ps. Following equilibration, NVE simulations of 100 ps were performed. All MB-MD simulations using MB-pol were run with a modified version of the DL_POLY 2.0 molecular dynamics package (45). Periodic boundary conditions were used in all cases, with a box size of 100 × 100 × 100 Å. The velocity Verlet algorithm was used to integrate Newton's equations of motions with a time step of 0.2 fs. The "always stable predictor corrector" method was used for the calculation of induced dipoles during the MB-MD simulations. Nosé–Hoover chains of 4 beads attached to each degree of freedom were used to control the temperature.

Data Availability. Experimental data and simulation results like geometries of cluster structures will be provided in electronic form upon request (please contact the corresponding authors V.M., F.P., or T.Z.). The procedures of experiments and simulations are described in detail in *Materials and Methods* and in *SI Appendix*. Please contact us when further information is needed to build on this work. We provide long-term availability of the data using the data storage infrastructure of our institutions.

ACKNOWLEDGMENTS. D.R.M., A.H., F.P., and V.M. were supported by NSF Award CHE-1305427. T.Z. was supported by Deutsche Forschungsgemeinschaft Grants ZE890 1-2 (No. 143238629) and 4-1 (No. 400183980). All calculations with the MB-pol water model used resources of the Extreme Science and Engineering Discovery Environment 107, which is supported by NSF Grant ACI-1053575. T.Z. thanks Prof. Martin Suhm for continuous support. U.B. and T.Z. thank Prof. Jim Lisy for valuable hints. F.Z. thanks the Heinrich Böll Stiftung and D.B. thanks the Fonds der Chemischen Industrie for financial support. A.H. and V.M. thank the Center for High Performance Computing at The University of Utah for technical support and a grant of computing time.

1. G. Torchet, P. Schwartz, J. Farges, M. F. de Feraudy, B. Raoult, Structure of solid water clusters formed in a free jet expansion. *J. Chem. Phys.* **79**, 6196–6202 (1983).
2. C. C. Pradzynski, R. M. Forck, T. Zeuch, P. Slavíček, U. Buck, A fully size-resolved perspective on the crystallization of water clusters. *Science* **337**, 1529–1532 (2012).
3. R. J. Cooper, M. J. DiTucci, T. M. Chang, E. R. Williams, Delayed onset of crystallinity in ion-containing aqueous nanodrops. *J. Am. Chem. Soc.* **138**, 96–99 (2016).
4. V. Buch, S. Bauerecker, J. P. Devlin, U. Buck, J. K. Kazimirski, Solid water clusters in the size range of tens—thousands of H_2O: A combined computational/spectroscopic outlook. *Int. Rev. Phys. Chem.* **23**, 375–433 (2004).
5. B. Bandow, B. Hartke, Larger water clusters with edges and corners on their way to ice: Structural trends elucidated with an improved parallel evolutionary algorithm. *J. Phys. Chem. A* **110**, 5809–5822 (2006).
6. J. C. Johnston, V. Molinero, Crystallization, melting, and structure of water nanoparticles at atmospherically relevant temperatures. *J. Am. Chem. Soc.* **134**, 6650–6659 (2012).
7. K. Liu *et al.*, Characterization of a cage form of the water hexamer. *Nature* **381**, 501–503 (2006).
8. J. D. Cruzan *et al.*, Quantifying hydrogen bond cooperativity in water: VRT spectroscopy of the water tetramer. *Science* **271**, 59–61 (1996).
9. C. J. Gruenloh *et al.*, Infrared spectrum of a molecular ice cube: The S_4 and D_{2d} water octamers in benzene-$(water)_8$. *Science* **276**, 1678–1681 (1997).
10. U. Buck, I. Ettischer, M. Melzer, V. Buch, J. Sadlej, Structure and spectra of three-dimensional $(H_2O)_n$ clusters, n = 8, 9, 10. *Phys. Rev. Lett.* **80**, 2578–2581 (1998).
11. K. Nauta, R. E. Miller, Formation of cyclic water hexamer in liquid helium: The smallest piece of ice. *Science* **287**, 293–295 (2000).
12. C. Perez *et al.*, Structures of cage, prism, and book isomers of water hexamer from broadband rotational spectroscopy. *Science* **336**, 897–901 (2012).
13. U. Buck, C. C. Pradzynski, T. Zeuch, J. M. Dieterich, B. Hartke, A size resolved investigation of large water clusters. *Phys. Chem. Chem. Phys.* **16**, 6859–6871 (2014).
14. S. E. Brown *et al.*, Monitoring water clusters "melt" through vibrational spectroscopy. *J. Am. Chem. Soc.* **139**, 7082–7088 (2017).
15. J. Brudermann, U. Buck, V. Buch, Isomerization and melting-like transition of size-selected water nonamers. *J. Phys. Chem. A* **106**, 453–457 (2002).
16. D. Laria, J. Rodriguez, C. Dellago, D. Chandler, Dynamical aspects of isomerization and melting transitions in $(H_2O)_8$. *J. Phys. Chem. A* **105**, 2646–2651 (2001).
17. C. C. Pradzynski *et al.*, Infrared detection of $(H_2O)_{20}$ isomers of exceptional stability: A drop-like and a face-sharing pentagonal prism cluster. *Phys. Chem. Chem. Phys.* **16**, 26691–26696 (2014).
18. S. W. Lee, P. Freivogel, T. Schindler, J. L. Beauchamp, Freeze-dried biomolecules: FT-ICR studies of the specific solvation of functional groups and clathrate formation observed by the slow evaporation of water from hydrated peptides and model compounds in the gas phase. *J. Am. Chem. Soc.* **120**, 11758–11765 (1998).
19. L. Ma, K. Majer, F. Chirot, B. von Issendorff, Low temperature photoelectron spectra of water cluster anions. *J. Chem. Phys.* **131**, 144303 (2009).
20. S. Kazachenko, A. J. Thakkar, Water nanodroplets: Predictions of five model potentials. *J. Chem. Phys.* **138**, 194302 (2013).
21. F. Zurheide *et al.*, Size-resolved infrared spectroscopic study of structural transitions in sodium-doped $(H_2O)_n$ clusters containing 10-100 water molecules. *J. Phys. Chem. A* **119**, 2709–2720 (2015).
22. A. Manka *et al.*, Freezing water in no-man's land. *Phys. Chem. Chem. Phys.* **14**, 4505–4516 (2012).
23. N. Gimelshein, S. Gimelshein, C. C. Pradzynski, T. Zeuch,U. Buck, The temperature and size distribution of large water clusters from a non-equilibrium model. *J. Chem. Phys.* **142**, 244305 (2015).
24. C. W. Dierking *et al.*, Revealing isomerism in sodium-water clusters: Photoionization spectra of $Na(H_2O)_n$ (n = 2-90). *J. Chem. Phys.* **146**, 244303 (2017).
25. J. P. Devlin, V. Buch, Surface of ice as viewed from combined spectroscopic and computer modeling studies. *J. Phys. Chem.* **99**, 16534–16548 (1995).
26. G. A. Cisneros *et al.*, Modeling molecular interactions in water: From pairwise to many-body potential energy functions. *Chem. Rev.* **116**, 7501–7528 (2016).
27. V. Babin, C. Leforestier, F. Paesani, Development of a "first principles" water potential with flexible monomers: Dimer potential energy surface, VRT spectrum, and second virial coefficient. *J. Chem. Theory Comput.* **9**, 5395–5403 (2013).
28. V. Babin, G. R. Medders, F. Paesani, Development of a "first principles" water potential with flexible monomers. II: Trimer potential energy surface, third virial coefficient, and small clusters. *J. Chem. Theory Comput.* **10**, 1599–1607 (2014).
29. G. R. Medders, V. Babin, F. Paesani, Development of a "first-principles" water potential with flexible monomers. III. liquid phase properties. *J. Chem. Theory Comput.* **10**, 2906–2910 (2014).
30. S.K. Reddy, D. R. Moberg, S. C. Straight, F. Paesani, Temperature-dependent vibrational spectra and structure of liquid water from classical and quantum simulations with the MB-pol potential energy function. *J. Chem. Phys.* **147**, 244504 (2017).
31. D. R. Moberg, S. C. Straight, F. Paesani, Temperature dependence of the air/water interface revealed by polarization sensitive sum-frequency generation spectroscopy. *J. Phys. Chem. B* **122**, 4356–4365 (2018).
32. V. Molinero, E. B. Moore, Water modeled as an intermediate element between carbon and silicon. *J. Phys. Chem. B* **113**, 4008–4016 (2009).
33. A. H. Nguyen, V. Molinero, Identification of clathrate hydrates, hexagonal ice, cubic ice, and liquid water in simulations: The CHILL+ algorithm. *J. Phys. Chem. B* **119**, 9369–9376 (2015).
34. K. Mizuse, N. Mikami, A. Fujii, Infrared spectra and hydrogen-bonded network structures of large protonated water clusters $H^+(H_2O)_n$ ($n = 20 - 200$). *Angew. Chem. Intl. Ed.* **49**, 10119–10122 (2010).
35. M. Born, K. Huang, *Dynamical Theory of Crystal Lattices* (Clarendon Press, Oxford, UK, 1954).
36. P. Carrier, R. Wentzcovitch, J. Tsuchiya, First-principles prediction of crystal structures at high temperatures using the quasiharmonic approximation. *Phys. Rev. B* **76**, 064116 (2007).
37. P. Varilly, D. Chandler, Water evaporation: A transition path sampling study. *J. Phys. Chem. B* **117**, 1419–1428 (2013).

38. C. Hock *et al.*, Calorimetric observation of the melting of free water nanoparticles at cryogenic temperatures. *Phys. Rev. Lett.* **103**, 073401 (2009).
39. N. Kastelowitz, V. Molinero, Ice-liquid oscillations in nanoconfined water. *ACS Nano* **12**, 8234–8239 (2018).
40. J. Jellinek, T. L. Beck, R. S. Berry, Solid-liquid phase changes in simulated isoenergetic Ar_{13}. *J. Chem. Phys.* **84**, 2783–2794 (1986).
41. S. Plimpton, Fast parallel algorithms for short-range molecular dynamics. *J. Comput. Phys.* **117**, 1–19 (1995).
42. G. J. Martyna, M. L. Klein, M. Tuckerman, Nosé-Hoover chains: The canonical ensemble via continuous dynamics. *J. Chem. Phys.* **97**, 2635–2643 (1992).
43. S. Nosé, A unified formulation of the constant temperature molecular dynamics methods. *J. Chem. Phys.* **81**, 511–519 (1984).
44. W. G. Hoover, Canonical dynamics: Equilibrium phase-space distributions. *Phys. Rev. A* **31**, 1695–1697 (1985).
45. W. Smith, C. W. Yong, P. M. Rodger, DL_POLY: Application to molecular simulation. *Mol. Sim.* **28**, 385–471 (2002).